Journal of Applied Electrochemistry **30**: 277–284, 2000.

Electrodeposition of Ni–Co alloys from sulfamate baths

S. GOLDBACH, R. de KERMADEC and F. LAPICQUE*
Laboratoire des Sciences du Génie Chimique, CNRS–ENSIC, BP 451, F-54001 Nancy, France
*(*author for correspondence, e-mail: lapicque@ensic.u-nancy.fr; fax: +33 3 83322975)*

Received 28 June 1999; accepted in revised form 28 September 1999

Key words: galvanostatic deposition, impedance spectrocopy, nickel–cobalt electrodeposition, rotating cylinder hull cell, sulfamate bath

Abstract

The paper describes the results of electrochemical investigations of Ni–Co deposition from a sulfamate bath in the presence of boric acid and two additives. The individual deposition of nickel was shown to be partly inhibited by the adsorption of sulfamate ions at low polarization; such inhibition was not observed for cobalt. The introduction of saccharin at 100 ppm, with a wetting agent seems to hinder sulfamate adsorption and Ni deposition departs at less cathodic potentials. The presence of cobalt has no effect on nickel deposition, whereas cobalt deposition is hindered by the presence of nickel in the bath. Galvanostatic deposition was carried out at the surface of a RDE and with a rotating cylinder Hull cell. At low current densities deposits with a Co content of approx. 40% were produced, but this content was shown to decrease with the applied current density. Examination of experimental data showed that cobalt deposition is diffusion-controlled and that Co content decreases with the applied current density relative to the limiting current density.

List of symbols

C_b	bulk concentration (mol m^{-3} or M)
C_{dl}	double layer capacitance (μF cm^{-2})
D	diffusion coefficient (m^2 s^{-1})
E	electrode potential (V)
F	Faraday constant (96 487 A s equiv.$^{-1}$)
h_c	length of the rotating cylinder (m)
i_{av}	average current density (A m^{-2})
i_L	limiting current density (A m^{-2})
i	current density (A m^{-2})
n_e	number of electrons involved in the reaction
n	impedance parameter for the constant phase element
r_c	diameter of the rotating cylinder (m)
x	coordinate along the cylinder (m)

Greek letters

β	Tafel constant (V^{-1})
δ	dimensionless average current density introduced in [22]
κ	electrical conductivity (Ω^{-1} m^{-1})
ν	kinematic viscosity (m^2 s^{-1})
ω	rotation rate (rad s^{-1})

1. Introduction

The electrodeposition of alloys of iron-group metals has been intensively investigated for decades because of their particular magnetic and mechanical properties in numerous applications in industry. Due to its low cost compared with cobalt, iron has been preferred for the production of Ni-based alloys. However, the presence of cobalt in nickel alloys is known to improve the hardness of the solid [1–3]. Additives such as saccharine or wetting agents have been used for years to reduce internal stresses in the material deposited [3, 4]. Ni–Co alloys with high mechanical properties can be produced by electrodeposition at well-defined conditions of temperature, pH, and current density [5]. Microfabrication by the LIGA process and using Ni–Co alloy was reported in [6].

The electrodeposition of nickel alloys from chloride or sulphate baths has been widely studied, and numerous contributions have dealt with its anomalous character allowing higher contents of the less noble metal (iron or cobalt) in the deposit than in the bath [7–9]. Sulfamate baths are often preferred to chloride or sulfate in the plating industry because of their high solubility [1, 3, 5], enabling high current densities in the production lines. In addition, these baths are of excellent stability for pH ranging from 2 to 4 and for temperatures up to 60 °C [10, 11]. Most of the papers dealing with deposition from sulfamate baths describe the mechanical properties of the alloys produced [3] or the Co content in the deposit [1, 5], and the electrochemistry of the deposition has been scarcely investigated [4].

The present work was aimed at investigating Ni–Co deposition from a sulfamate bath with a Ni:Co ratio of the order of 10 and in the presence of boric acid and two additives. Such a bath has been used by Robert Bosch GmbH, Stuttgart, Germany, in galvanic processes on patterned electrodes [12]. Polarization curves and impedance measurements were carried out to highlight the deposition and the results obtained were discussed in comparison with published data related to deposition from other baths. Galvanostatic deposition was carried out on the surface of a rotating disc electrode, RDE, and in a rotating cylinder Hull cell, RCH cell: the Co content in the deposit was correlated with the applied cd relative to the limiting current density.

2. Experimental section

2.1. *Chemicals*

Alloy deposition was investigated from an industrial bath containing sulfamate salts of nickel and cobalt, at 76 g l^{-1} and 7 g l^{-1} of the two metal cations, respectively. Nickel and cobalt sulfamates in the form of concentrated solutions, were purchased from Candorchemie (Bochum, Germany) and Blasberg (Solingen, Germany), respectively. Boric acid (Prolabo, France) was introduced at 35 g l^{-1} for all experiments. Two additives were used simultaneously in the solution at 100 ppm each: saccharin, in the form of sodium salt (Prolabo, France), and FC 95^{TM} (3M, The Netherlands). The latter additive is a blend of sodium salts of fluoroalkylsulfonate exhibiting effective wetting properties. The bath pH was carefully controlled and adjusted to 4.0 within 0.1 by addition of sulfamic acid or sodium hydroxide. Temperature was fixed at 50 °C as in the industrial process in Stuttgart, allowing sufficient solubility of boric acid and high stability of sulfamate ion. The viscosity of the Ni–Co electrolytic bath, ν, was measured at 1.02×10^{-6} m^2 s^{-1} at 50 °C using an Ubbelhode viscometer.

2.2. *Polarization curves*

i/E curves were recorded at steady state or by continuous sweeping of the potential of the RDE (EG&G Princeton Applied Research 616), with a rotation rate ranging from 200 to 1000 rpm. The disc electrode was a titanium piece 4.0 mm in diameter embedded into a 12 mm PTFE cylinder. The electrode was polished with emery paper and diamond paste, then rinsed with distilled water. A predeposit was prepared on the substrate surface from the considered electrolytic bath at 100 A m^{-2} for one minute. All potentials were referred to the saturated calomel electrode (SCE). The counter electrode was a basket 40 mm in diameter out of nickel for Ni and Ni–Co deposition, and cobalt for Co deposition. The three electrodes were immersed in a 400 cm^3 glass cell provided with a water jacket for temperature control.

All experiments were carried out with a EG&G 273 A potentiostat. Impedance measurements were done with a frequency analyser (Schlumberger SI 1255) connected to the potentiostat. Potential varied with an amplitude of 5 mV around its steady value and the frequency varied from 10^{-3} to 10^5 Hz.

2.3. *Galvanostatic deposition*

Galvanostatic experiments were carried out at the surface of a rotating disc electrode, or in a rotating cylinder Hull cell, as developed by Madore et al. [13]. The design of the cell was derived from that suggested by Madore and Landolt [14]. The cell consisted of a cylindrical vessel, 150 mm high and 130 mm in diameter. The working electrode was a titanium piece (60 mm long × 15 mm dia.) fixed on a cylindrical PTFE shaft; 7.5 mm recesses at the electrode extremities prevented edge effects. The electrode-shaft assembly was screwed to the EG&G motor, enabling both its regular rotation and electrical connection to the potentiostat. The counter electrode was a sacrificial anode consisting of a nickel cylinder inserted close to the inner wall of the cell. A stationary, concentric tube, (85 mm long × 55 mm inner dia.) was inserted between the two electrodes and allowed a large variation of the primary distribution of current [13].

Deposition runs in the RCH cell were carried out for 5–40 min depending on the applied current, and the weight of the produced deposit was of the order of 150 mg.

Deposits prepared on the RCH cell cylinder and at the RDE surface were dissolved in concentrated nitric acid. The acidic phase recovered was diluted with water and assayed by atomic absorption (Varian AA 20), yielding the weight contents of the two metals in the alloy. The composition of the deposit prepared on the cylinder electrode was determined as a function of the axial location as follows. The cylinder surface was divided into twelve cylindrical elements, each being 5 mm high: the deposit on each element was dissolved and analysed separately, allowing the distribution of metal contents to be determined along the electrode length. The sum of the amounts of metal yielded by the experimental procedure corresponded usually to more than 90% of the weight of metal expected from the electrical charge passed.

Nickel dissolution occurred on the sacrificial anode of the RCH cell, whereas Ni–Co alloy was deposited at the rotating cathode. The resulting change in metal concentration was thoroughly followed by regular analysis of the bath. The composition of the bath was maintained as constant as possible by renewal of the solution and addition of cobalt sulfamate: for all experiments reported here, the molar ratio Ni/Co in the electrolytic bath was 10.8 ± 0.5.

3. Polarization curves

Individual depositions of nickel and cobalt, from baths at 76 g l^{-1} and 7 g l^{-1} of metal respectively, were studied prior to codeposition from the bath presented above.

Polarization curves were obtained at steady-state by measurements of the RDE potential at fixed current: the time required for each measurement usually ranged from 10 s to 1 min. Potential was corrected for ohmic drop, assuming that the reference electrode was very far from the RDE surface and using the cell resistance measured by impedance spectroscopy. This resistance was measured at 14 Ω for the Ni–Co containing bath. The baths used for investigation of the individual depositions had a resistance of 15 Ω for nickel sulfamate at 76 g l^{-1}, and 66 Ω for cobalt sulfamate at 7 g l^{-1}.

After a series of measurements, the electrode surface was renewed by dissolution of the deposit and preparation of a fresh predeposit. Voltammetric curves were also recorded with scanning rates ranging from 1 to 10 mV s^{-1}: the curves obtained by continuous sweeping of the potential were of moderate reproducibility and could differ to a significant extent from the steady-state measurements, especially for the case of deposition of pure nickel. Only the results of steady polarization are presented here.

3.1. *Nickel deposition*

In the absence of additives, i/E curves of Ni deposition exhibited only one region in Tafel plot for cd in the range 10–1000 A m^{-2}. Rotation rate had a small influence on the curve and, as reported in previous papers ([15] for instance), higher currents were allowed at lower rotation rates for low to moderate polarization of the electrode. Reduction of Ni^{2+} ion from the sulfamate bath started at potentials nearly 300 mV more cathodic than the standard potential at −0.254 V vs NHE. The reduction appeared to be retarded in comparison with depositions from sulphate or chloride baths (Figure 1): at moderate c.d., the measured voltage was nearly 100 mV more cathodic than from the Watts-type bath used by Epelboin and Wiart [16] at the same temperature. The low activation of nickel deposition may be due to sulfamate adsorption at the surface of the weakly polarised electrode. Over −1.25 V vs SSCE, the deposition occurred with a Tafel constant of 25.5 V^{-1}, in fair agreement with the constants reported by Fan and Piron [17] of 25.9 V^{-1}, however from a chloride bath at 25 °C. The value obtained can also be compared with the first Tafel constant reported [16] of 23 V^{-1}, or by Madore and Landolt [18], of 28 V^{-1}.

Polarization curves recorded in the presence of the two additives presented two linear domains, as in previous investigations: at low polarization, the Tafel constant b_1 was near 28 V^{-1}, whereas b_2, for c.d. over 500 A m^{-2}, was estimated at 16.5 V^{-1}. Surprisingly, the simultaneous presence of the additives allowed Ni deposition to depart at less cathodic potentials (Figure 2), whereas most additives, for examples, saccharine, butyne-diol, coumarine or sodium sulphonate, when present in sulphate or chloride baths, were shown to retard the deposition. For the present case, it may be assumed that the additives, although adsorbing on the surface, reduce the inhibiting behaviour of sulfamate ions and favour the access of Ni^{2+} to the electrode.

3.2. *Cobalt deposition*

Cobalt deposition occurred at potentials less cathodic than Ni^{2+} reduction and the inhibiting effect of sulfamate was not observed. Polarization curves from the 0.13 M cobalt salt solution were little affected by the presence of the additives (Figure 3). As a matter of fact, the potential recorded at given c.d. from the additive-free bath differed by less than 10 mV from that with the second bath. The reduction mechanism and the role of the additive seem to be different from those for Ni deposition. The curves shown in Figure 3 exhibit Tafel behaviour with a constant at 30.0 V^{-1}, that is 77 mV (decade)$^{-1}$, for c.d. up to 1500 A m^{-2}. The constant value is noticeably above that obtained by [17] with a chloride bath at 25 °C. Increasing further the cathode polarization resulted in levelling-off of the

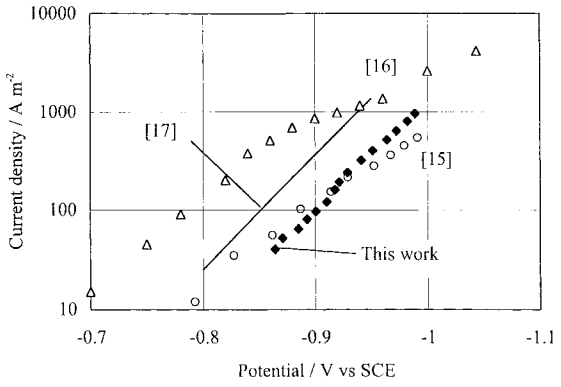

Fig. 1. Steady-state polarization curves of nickel deposition from additive-free bath: comparison with published data with other baths.

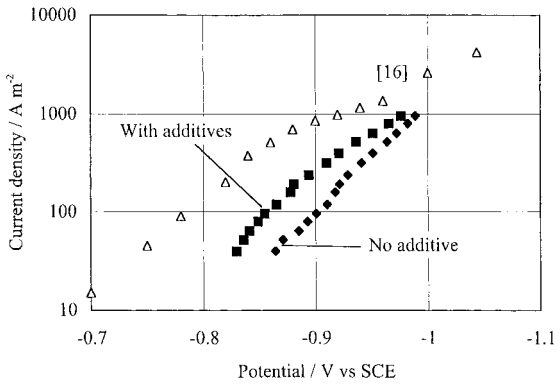

Fig 2. Steady-state polarization curves of nickel deposition: effect of the additives and comparison with data reported in [15] (additive-free sulphate bath at 50 °C).

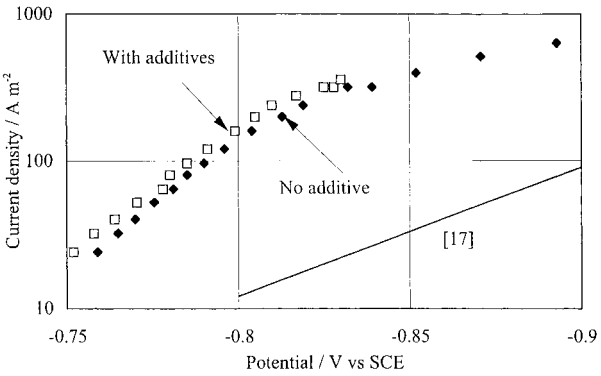

Fig. 3. Steady-state polarization curves of cobalt deposition and effect of the two additives.

current variation, attributable to significant control by diffusion.

3.3. *Ni–Co alloy deposition*

Figure 4 shows the results of steady polarization, together with the i/E variations obtained for galvanostatic runs carried out on the RDE, varying the rotation rate and the applied current (Section 6). The two sources of data were consistent and the overall i/E variation exhibited two regions (Figure 4). Below 200 A m^{-2}, current density increased rapidly with overpotential with a polarization constant near 27 V^{-1}, that is 85 mV/(decade)$^{-1}$. For higher c.d., polarization became slower and the slope of the second asymptote was of the order of 15 V^{-1}. The current recorded differed considerably from the sum of the currents for the individual depositions carried out with the two additives. In the potential range investigated, -0.8 V to -1.1 V vs SCE, the current for Co individual deposition was quite higher than that of the alloy deposition, which lay close to that of Ni individual deposition.

Analysis of the alloy deposits produced by galvanostatic runs on the RDE yielded currents for the partial depositions of nickel and cobalt, depending on the applied current. For nickel, the two current variations are fairly close, as shown in Figure 5, and it can be concluded that nickel deposition from sulfamate baths is little affected by the presence of cobalt. In contrast, the current density of cobalt partial deposition was found to be significantly lower than that of individual deposition: cobalt deposition, being less inhibited by sulfamate ion than nickel deposition, appears to be inhibited by the presence of nickel for the alloy deposition.

This result is in contradiction with published work [9, 19], which showed significant inhibition of nickel by an adsorbed reaction intermediate of the less noble metal: codepositing metals from sulphate baths lowers the partial current of nickel. For the present case, due to the inhibiting behaviour of sulfamate species, even in the presence of additives, nickel deposition seems to be unaffected by the presence of cobalt.

4. Impedance spectroscopy

For low polarization of the electrode surface, i.e. for c.d. below 1 A m^{-2}, no reproducible spectra of individual depositions or alloy production could be recorded, and this may be attributed to the likely inhibition by sulfamate species. For current densities of the order of 10 A m^{-2}, spectra exhibited one capacitive loop in a large frequency domain that could be fitted by the CPE model [20]: fit was of an acceptable accuracy for Ni and Ni–Co alloy deposition, whereas the loop relative to Co deposition was distorted, with imaginary parts lower than expected at low frequency. For the three reductions and at low c.d., parameter n was usually determined below 0.8, expressing the complex state of the electrode surface. Increasing the absolute potential resulted in more regular spectra with higher n values. Over 100 A m^{-2}, spectra consisted of a large capacitive loop, with n at unity within a few percent, followed by another feature at low frequencies depending on the composition of the electrolytic bath. In this c.d. range, the double

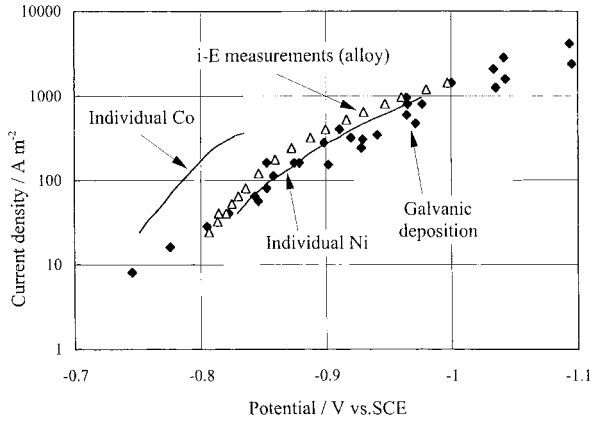

Fig. 4. i/E curves of nickel–cobalt codeposition with additives: comparison of steady-state polarization with the current measured for galvanostatic experiments. The i/E curves for the individual depositions of nickel and cobalt are also given.

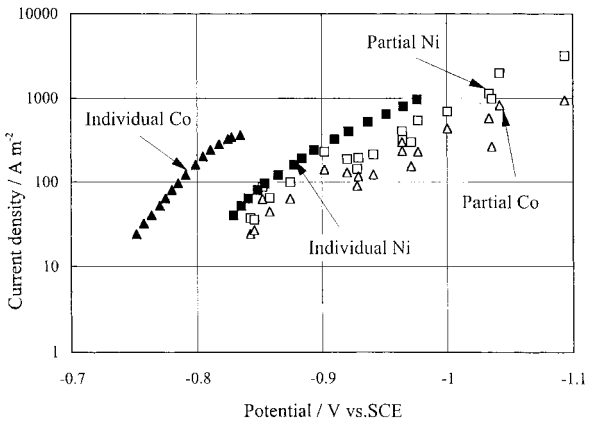

Fig. 5. i/E curves of metal deposition with additives: comparison of the currents for the individual depositions with the partial current of Ni and Co deposition during galvanostatic experiments.

layer capacitance was deduced from the high frequency loop using the simple model of irreversible electron transfer.

4.1. *Nickel deposition*

In additive-free solution, the low frequency feature was an inductive loop as shown in Figure 7. Similar spectra observed by Epelboin and Wiart [16] with a Watts-type bath, were attributed to the adsorption of intermediate NiOH. However, the existence of the intermediate was not suggested by a change in the Tafel slope (Figure 1). The double layer capacitance was of the order of 50 μF cm^{-2}, indicating that the cathode surface was accessible to Ni^{2+} reduction, at least for sufficient overvoltages.

The presence of additives changed the impedance spectra (Figure 6). First, the double layer capacitance was noticeably reduced at 35 μF cm^{-2}, in agreement with previous observations with other additives [15]. The low frequency part of the spectra consisted of a small inductive loop followed by a second capacitive loop, for frequencies below 1 Hz. The difference in the low frequency region might be due to the adsorption of the additives.

4.2. *Ni–Co alloy deposition*

Examples of impedance spectra for the alloy deposition are given in Figure 7, depending on current density. The capacitance was found to be 45 μF cm^{-2} within 5 μF cm^{-2} for current densities ranging from 70 to 300 A m^{-2}. The capacitive loop ended on the real axis for frequencies varying from 10 Hz at 84 A m^{-2} to 100 Hz at 240 A m^{-2}. Below the above frequencies, the electrode impedance remained fairly constant, with an insignificant imaginary part, and an inductive loop was observed below 0.03 Hz. This well-defined loop observed at moderate c.d., became less significant at higher

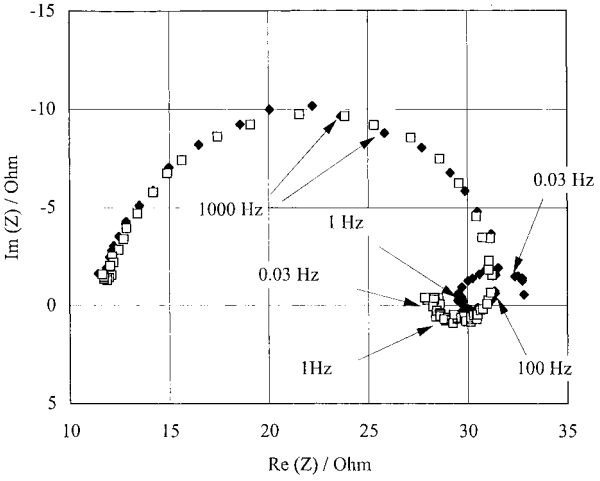

Fig. 6. Impedance spectra of nickel deposition at 240 A m^{-2}, with additives (◆) or without (□).

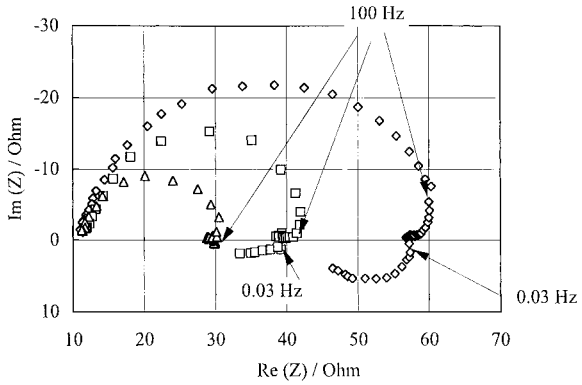

Fig. 7. Impedance spectra of Ni–Co deposition with additives at various current densities: (◇) 90 (□) 160 and (△) 250 A m^{-2}.

polarization, and was no longer visible over 200 A m^{-2}. This phenomenon which may be linked to the rate-controlling formation of the adsorbed intermediate at moderate c.d., is consistent with Epelboin and Wiart's observations, however, for single-metal deposition. The low frequency features differed from those for Ni deposition with additives which remained significant at high current densities (Figure 6).

5. Current distributions in the rotating cylinder Hull cell

Current distributions along the rotating cylinder are governed by the design of the cell, and in particular by the presence of the inert baffle placed between anode and cathode. The primary c.d. distribution in Madore's cell, with the anode placed at one cell extremity, was fitted by the following law [13]:

$$\frac{i(x/h_c)}{i_{av}} = \frac{0.535 - 0.458(x/h_c)}{\sqrt{0.023 + (x/h_c)^2}} + 8.52 \times 10^{-5} \exp\left(7.17 \frac{x}{h_c}\right) \quad (1)$$

where h_c is the length of the active cylinder, x is the coordinate from the upper edge of the cylinder, and i_{av} is the average current density. Primary distribution in the cell shown in Figure 8 was calculated by numerical integration of Laplace equation using Cell-Design software. The two primary distributions were shown to differ by only a few percents (Figure 8). For the present study, the ratio $(i(x/h_c)/i_{av})$ varied from 3.433 at the upper edge, to 0.122 at the lower edge.

Current distributions on the rotating cylinder are to be affected by charge transfer resistance and formation of concentration profiles near the electrode surface at sufficient polarization.

5.1. *Estimation of the limiting current density*

The rotating Hull cell is usually operated in turbulent regime, that is, for Reynolds number over 200 [14]:

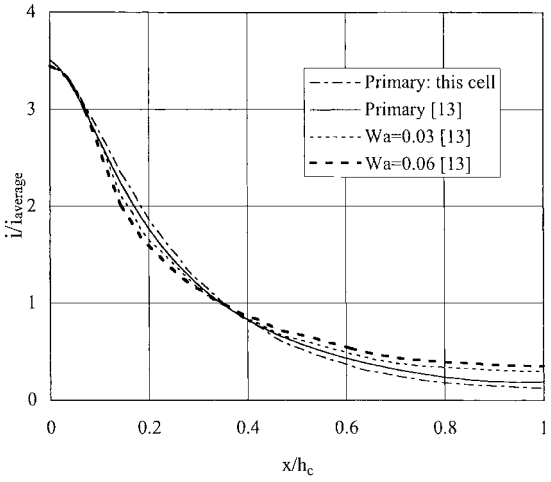

Fig. 8. Theoretical primary and secondary distributions of current in the rotating cylinder Hull cell.

$$\frac{\omega r_c^2}{\nu} > 200 \tag{2}$$

where r_c is the cylinder diameter. In the present case, Relation 2 holds for rotation speeds, N, over 35 rpm. The limiting current density for a single electrochemical process can be estimated from Eisenberg's relationship [21]:

$$i_L = 0.079\, n_e\, F C_b (2\,\omega r_c) \left(\frac{2\,\omega r_c^2}{\nu}\right)^{-0.3} \left(\frac{\nu}{D}\right)^{-0.644} \tag{3}$$

where C_b is the bulk concentration of the electroactive species and D its diffusion coefficient. The limiting current for alloy deposition is not straightforward: cobalt is expected to be deposited under diffusion control at sufficient polarization, whereas nickel deposition is kinetically controlled. However, the applied current density can be compared with a theoretical limiting c.d. which may be defined arbitrarily as the limiting c.d. for Ni deposition, because of the high Ni/Co molar ratio in the bath. Its value was estimated with C_b at 1300 mol m^{-3} and a diffusion coefficient assumed at 5×10^{-10} m^2 s^{-1} at 50 °C. Rotation rate was varied from 35 to 935 rpm, corresponding to i_L variation from 800 to 8150 A m^{-2}.

5.2. *Range of current density*

The current to be applied to the cell was fixed so that the local cd was below the estimated limiting c.d. i_L along the cylinder: the primary current distribution yielded the following constraint for i_{av}:

$$3.433\, i_{av} < i_L \tag{4}$$

Relation 4 relies upon several approximations: first, i_L represents only an estimate for the limiting current density, and the occurrence of hydrogen evolution may be expected beyond this limit. In addition, the maximal current density at the cathode surface may differ from the theoretical value ($3.433\, i_{av}$) calculated for the primary distribution. The current density applied to the rotating cylinder was therefore varied from 59 to 908 A m^{-2}, depending on the rotation rate.

Secondary distributions in a rotating cylinder Hull cell were calculated by Madore et al. [13], depending on the Wagner number defined on the cylinder length as follows:

$$Wa = \frac{\kappa}{\beta i_{av} h_c} \tag{5}$$

where κ is the bath conductivity, determined as 8.9 Ω^{-1} m^{-1} at 50 °C from the cell resistance and use of Newman's relation for the ohmic drop at infinite distance from a RDE surface. The c.d. range considered led to *Wa* values lying from 0.008 to 0.093. The effect of charge transfer resistance in Madore's cell is exemplified in Figure 8 for *Wa* at 0.06: as expected the distribution was more even and the reduced current density attained 0.33 at the lower edge. Nevertheless, the distribution was little affected by charge transfer resistance on the upper millimetres of the cylinder.

5.3. *Current distributions*

Deposition experiments carried out on the surface of the rotating cylinder were interpreted in terms of current density depending on x coordinate: analysis of the deposit at location x yielded the partial current densities for cobalt and nickel deposition. The sum of partial c.d. was compared with theoretical primary and secondary distributions, and two examples are given in Figure 9 for *Wa* near 0.03. The experimental variations were in good agreement with the secondary distribution calculated for $Wa = 0.03$ [13]. This confirmed that the current yield for the codeposition was close to unity, in agreement with alloy deposition runs on larger electrodes [12]. However, significant deviation was observed for the two upper segments, at $x = 2.5$ and 7.5 mm, for which the local cd was at its highest. This is particularly clear for an average c.d. at 75% of the ratio ($i_L/3.433$) (Figure 9(b)): although the local c.d. is below i_L, hydrogen evolution may occur and be the source of the difference between the experimental c.d. for alloy deposition and the theoretical predictions.

6. Cobalt content in the deposit

Galvanostatic deposition was carried out on the two rotating devices as a function of rotation rate and applied c.d. The limiting c.d. at the RDE surface was estimated using Levich law and with the same procedure as for the RCH cell (Section 5.1). Rotation rate of the disc electrode was varied from 100 and 2000 rpm and the current density relative to i_L lay between 0.01 and 0.80.

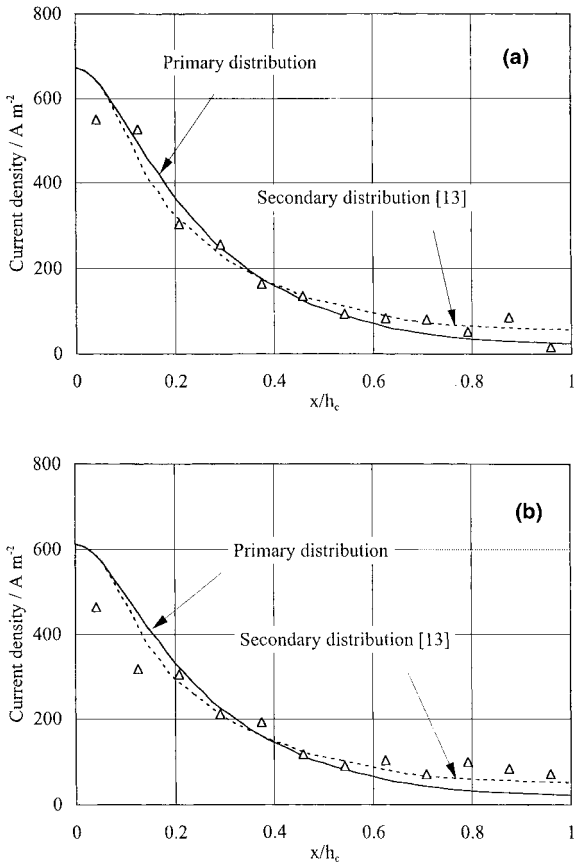

Fig. 9. Current distributions in the rotating cylinder Hull cell: comparison of experimental data for alloy deposition (△) with calculated primary and secondary distributions ($Wa = 0.03$ [13]). (a) i_{av} = 196 A m^{-2}, $i_L = 8123$ A m^{-2}, $Wa = 0.028$; (b) $i_{av} = 178$ A m^{-2}, i_L = 815 A m^{-2}, $Wa = 0.031$.

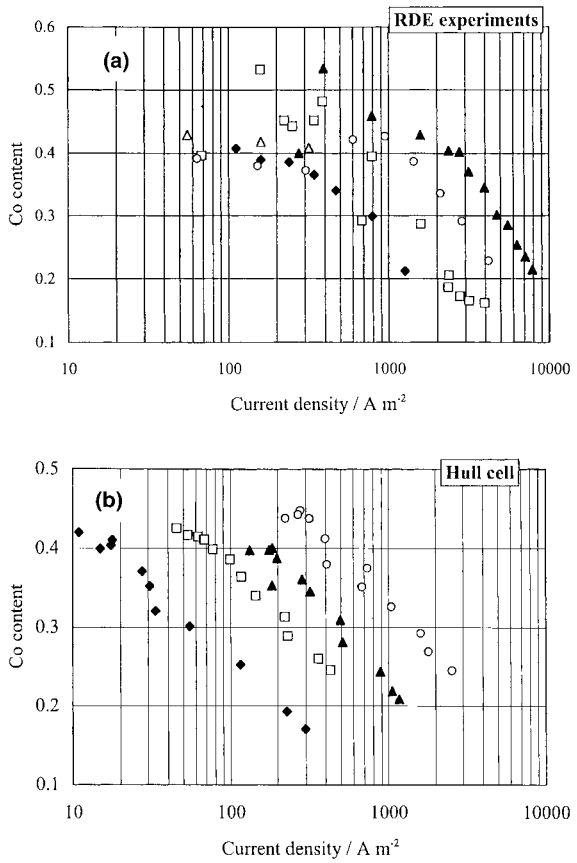

Fig. 10. Cobalt content in the alloy deposited against current density as a function of the rotating rate (in rpm). (a) RDE cell: (◆) 100, (□) 200, (△) 400, (○) 900 and (▲) 2000 rpm; (b) RCH Cell : (◆) 35, (□) 94, (▲) 253 and (○) 681 rpm.

For the two rotating electrodes investigated the alloy deposition was anomalous in the whole range of the current ratio i/i_L, and normal deposition could have been observed only for lower polarization. At given rotation rate the cobalt content was found to be of the order of 40 wt.% for low current densities, as shown in Figure 10 (a) and (b). Increasing the applied c.d. resulted in regular decrease of the cobalt content and the variation was nearly linear in semi-logarithmic plot. The cobalt content is in the range 16–22% for the highest polarization of the electrode. The decrease confirmed the control of cobalt deposition by mass transfer, reported previously with other electrolytic baths [17, 19]. The current density corresponding to the transition in Co content, depended on the rate of the two rotating devices: changing the rotation rate resulted in a horizontal shift in the variation with c.d. in the semi-logarithmic plot (Figure 10).

The data produced with the two electrodes were correlated by plotting the cobalt content against the c.d. ratio (i/i_L), and the plot shown in Figure 11 led to the following observations. For c.d. ratio (i/i_L) below 0.10, Co content remains roughly constant at 36–42%, due to the occurrence of anomalous deposition. Increasing polarization of the electrode results in regular decrease of Co content in the deposit. The values for Co content on the RDE surface seem to be slightly over those in the deposits produced on the rotating cylinder, with significant scattering. The differences between the two series of data may be related to nonuniform distribution of current on the disc surface: the moderate conductivity of the bath corresponds to high value of the dimensionless average current density, δ, introduced by Newman [22],

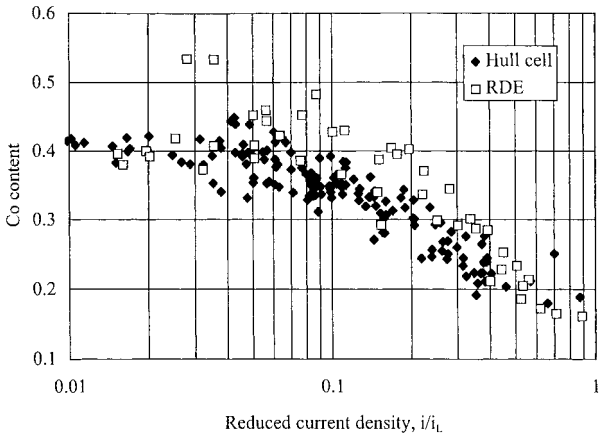

Fig. 11. Cobalt content against the reduced current density, i/i_L, at the two rotating electrodes; Ni/Co ratio in the bath was 10.8 ± 0.5.

with lower current densities and higher cobalt contents near the center of the disc than near the edges.

7. Conclusion

The electrochemistry of nickel–cobalt alloy deposition from sulfamate was shown to differ significantly from that of other baths such as chloride or sulfate solutions. Due to the complexing nature of sulfamate salts, nickel deposition is inhibited over an appreciable range of potential, and sulfamate ion likely adsorbs on the electrode surface for weak electrode polarization. It is postulated that the simultaneous presence of saccharin and FC95^{TM} wetting agent hinders sulfamate adsorption and favours Ni deposition, contrary to previous observations made with Watts baths. In the presence of the two additives, formation of an adsorbed NiOH intermediate may occur, as shown by polarization curves and impedance spectra at low frequency. The deposition of cobalt differs from that of nickel and seems to be less sensitive to the role of sulfamate.

Deposition of nickel from sulfamate bath for alloy deposition is little affected by the presence of cobalt, contrary to the behaviour in sulphate or chloride baths. On the contrary, polarization measurements showed that cobalt deposition is hindered by the presence of nickel, even though the alloy deposition is anomalous in a broad range of current density. Galvanostatic depositions of the alloy carried out on RDE surface and in a rotating cylinder Hull cell, suggested that cobalt deposition was a diffusion-controlled process, and that the cobalt content therefore decreased with the applied current density relative to the limiting current density.

The results can be used to determine the operating conditions of processes for Ni–Co deposition of well-controlled composition. The Co content in the alloy to be produced from a bath with a fixed Ni–Co ratio, can be estimated from the applied current density and mass transfer rates. In addition, electrolytic cells for this deposition should allow high mass transfer rates, with rate distributions as even as possible for the production of alloys of uniform composition and thickness on the whole surface of the substrate.

Acknowledgements

The authors are indebted to Dr Jacques Wijenberg, Hoogovens b.v., The Netherlands, for calculation of the primary distribution in the RCH Cell. This work was sponsored by the European Union in the frame of the Brite–Euram III programme BRPR-CT 95-0008.

References

1. D.W. Endicott and J.R. Knapp, *Plating* (Jan. 1966), 43.
2. W.H. Safranek, Nickel alloys, *in* 'The Properties of Electrodeposited Metals and Alloys – A Handbook' (Elsevier, New York, 1974).
3. S.A. Watson, 'Addition to sulfamate nickel solutions', NiDi Technical Series (1989) Nr. 10053.
4. R.J. Walter, *Plat. Surf. Finish.* (July 1980), 46.
5. H.U. Schwabe, *Industrie-Anzeiger 95*, **34** (1973) 703.
6. B. Löchel and A. Maciossek, *J. Electrochem. Soc.* **143** (1996) 3343.
7. A. Brenner, 'Electrodeposition of Alloys', Vols. 1 and 2, (Academic Press, New York 1963).
8. W. Grande and J.B. Talbot, *J. Electrochem. Soc.* **140** (1993) 679, 675.
9. M. Matlosz, *J. Electrochem. Soc.* **140** (1993) 2272.
10. J.L. Marti, *Plating* (Jan. 1966), 61–71.
11. H. Zhang and S.M. Park, *J. Appl. Electrochem.* **24** (1994) 1182.
12. Final report of the Brite-Euram III Programme, CT 95-0008 (Nov. 1998).
13. C. Madore, M. Matlosz and D. Landolt, *J. Appl. Electrochem.* **22** (1992) 1155.
14. C. Madore and D. Landolt, *Plat. Surf. Finish.* (Nov. 1993), 73–78.
15. C.C. Cheng and A. West, *J. Electrochem. Soc.* **144** (1997) 3050.
16. I. Epelboin and R. Wiart, *J. Electrochem. Soc.* **118** (1971) 1578.
17. C. Fan and D.L. Piron, *Electrochim. Acta* **41** (1996) 1713.
18. C. Madore and D. Landolt, *J. Electrochem. Soc.* **143** (1996) 3936.
19. N. Zech, J. Podlaha and D. Landolt, *J. Appl. Electrochem.* **28** (1998) 1251.
20. G.J. Brug, A.L.G. van den Eeden, M. Sluyters-Rehbach and J.H. Sluyters, *J. Electroanal. Chem.* **176** (1984) 275.
21. M. Eisenberg, C.W. Tobias and C.R. Wilke, *J. Electrochem. Soc.* **101** (1954) 306.
22. J. Newman, *J. Electrochem. Soc.* **113** (1966) 1235.